Self-nucleation and crystallization kinetics of double crystalline poly(*p*-dioxanone)-*b*-poly(ε-caprolactone) diblock copolymers†

Alejandro J. Müller,*[a] Julio Albuerne,[a] Leni Marquez,[a] Jean-Marie Raquez,[b] Philippe Degée,[b] Philippe Dubois,[b] Jamie Hobbs[c] and Ian W. Hamley[d]

[a] *Grupo de Polímeros USB, Departamento de Ciencia de los Materiales, Universidad Simón Bolívar, Apartado 89000, Caracas 1080-A, Venezuela. E-mail: amuller@usb.ve*
[b] *Laboratory of Polymeric and Composite Materials (LPCM), University of Mons-Hainaut, Place du Parc 20, 7000, Mons, Belgium*
[c] *Department of Chemistry, University of Sheffield, Sheffield S3 7HF, UK*
[d] *Department of Chemistry, University of Leeds, Leeds LS2 9JT, UK*

Received 1st March 2004, Accepted 4th April 2004
First published as an Advance Article on the web 17th August 2004

The crystallization kinetics of each constituent of poly(*p*-dioxanone)-*b*-poly(ε-caprolactone) diblock copolymers (PPDX-*b*-PCL) has been determined in a wide composition range by differential scanning calorimetry and compared to that of the equivalent homopolymers. Spherulitic growth rates were also measured by polarized optical microscopy while atomic force microscopy was employed to reveal the morphology of one selected diblock copolymer. It was found that crystallization drives structure formation and both components form lamellae within mixed spherulitic superstructures. The overall isothermal crystallization kinetics of the PPDX block at high temperatures, where the PCL is molten, was determined by accelerating the kinetics through a previous self-nucleation procedure. The application of the Lauritzen and Hoffman theory to overall growth rate data yielded successful results for PPDX and the diblock copolymers. The theory was applied to isothermal overall crystallization of previously self-nucleated PPDX (where growth should be the dominant factor if self-nucleation was effective) and the energetic parameters obtained were perfectly matched with those obtained from spherulitic growth rate data of neat PPDX. A quantitative estimate of the increase in the energy barrier for crystallization of the PPDX block, caused by the covalently bonded molten PCL as compared to homo-PPDX, was thus determined. This energy increase can dramatically reduce the crystallization rate of the PPDX block as compared to homo-PPDX. In the case of the PCL block, both the crystallization kinetics and the self-nucleation results indicate that the PPDX is able to nucleate the PCL within the copolymers and heterogeneous nucleation is always present regardless of composition. Finally, preliminary results on hydrolytic degradation showed that the presence of relatively small amounts of PCL within PPDX-*b*-PCL copolymers substantially retards hydrolytic degradation of the material in comparison to homo-PPDX. This increased resistance to hydrolysis is a complex function

† Electronic supplementary information (ESI) available: Video showing the sequential isothermal crystallization of $D_{23}^{8}C_{77}^{27}$ according to the same temperature program described in Fig. 2. See http://www.rsc.org/suppdata/fd/b4/b403085k/

of composition and its knowledge may allow future prediction of the lifetime of the material for biomedical applications.

Introduction

Poly(*p*-dioxanone), PPDX, and poly(ε-caprolactone), PCL, are considered as biocompatible and biodegradable materials suitable for biomedical applications in view of their molecular structures; their respective repeat units are shown in Scheme 1.

In particular PPDX applications include a series of bioabsorbable materials like sutures, pins for fracture fixation, surgical clips and fasteners. These applications are based on the relatively fast hydrolytic degradation of PPDX which can in some cases be too fast for certain biomedical applications. The idea to copolymerize it with PCL could provide a way to tune the lifetime of the biomedical devices within the human body since PCL hydrolytic degradation is several orders of magnitude lower than that of PPDX.[1,2]

Crystallization within block copolymer microdomains (MD) is an issue which has attracted increasing interest in recent years. The structure development in semicrystalline block copolymers depends on two competing self organizing mechanisms: microphase separation and crystallization. Depending on the segregation strength in the melt, crystallization can be either confined within the copolymer MD for strongly segregated systems, or crystallization can drive structure formation for weakly segregated melts (overwriting any previous MD) or homogeneous systems.

The most commonly studied of the semi-crystalline block copolymer systems in the literature have been AB diblock copolymers or ABA triblock copolymers where one block is amorphous and the other semicrystalline. It is generally accepted that the changes of state as a function of temperature can determine the final morphology according to three key transition temperatures: the order–disorder transition temperature T_{ODT}, the crystallization temperature (T_c) of the crystallisable block, and the glass transition temperature T_g of the amorphous block. A generalization can be made to describe four cases that have been described in the literature: (1) Homogeneous melt, $T_{ODT} < T_c > T_g$. In diblock copolymers exhibiting a homogeneous melt, microphase separation is driven by crystallization if T_g of the amorphous block is lower than the T_c of the crystallisable block. This generally results in a lamellar morphology where crystalline lamellae are sandwiched by the amorphous block layers and spherulite formation can be observed depending on composition.[3–7] (2) Weakly segregated systems, $T_{ODT} > T_c > T_g$ with soft confinement. In this case, crystallization often occurs with little morphological constraint enabling a ''breakout'' from the ordered melt structure and the crystallization overwrites any previous melt structure usually forming lamellar structures and in many cases spherulites depending on composition.[5,8–15] (3) Strongly segregated systems, $T_{ODT} > T_c > T_g$ with soft confinement. If the segregation strength is sufficiently strong, the crystallization can be confined within spherical, cylindrical or lamellar MD in strongly segregated systems with a rubbery block.[7,12–14,16–24] (4) Strongly segregated systems, $T_{ODT} > T_g > T_c$ with hard confinement. A strictly confined crystallization within MD has been observed for strongly segregated diblock copolymers with a glassy amorphous block.[25–38]

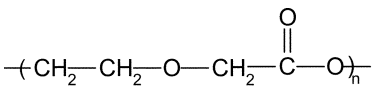

PPDX

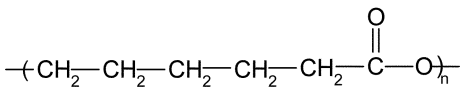

PCL

Scheme 1 Molecular structures of PPDX and PCL repeating units.

There have been relatively few reports dealing with double crystalline block copolymers.[39–45] The PPDX-*b*-PCL diblock copolymers have only been recently prepared[46] and we are unaware of other studies in similar materials except for the contribution of Lendlein and Langer[47] where multiblock copolymers of PPDX and PCL have been employed to prepare shape memory polymers for biomedical applications.

The objective of the present paper is to study the isothermal crystallization kinetics and self-nucleation of each one of the two constituents of the PPDX-*b*-PCL diblock copolymers as a function of composition. In this work, we have been able to follow the overall crystallization kinetics of the PPDX block by accelerating the overall crystallization rate through a self-nucleation procedure. The application of the Lauritzen and Hoffman theory to spherulitic growth rate data and to the overall crystallization data obtained after self-nucleation allowed us to calculate the energy barriers to crystal growth and to crystal nucleation. Using such a procedure, we were able to quantitatively estimate for the first time the effect of the molten PCL block on the energy barrier for crystallization of the PPDX block (melting points of PPDX and PCL are approximately 107 °C and 57 °C respectively). In the case of the PCL block, we first crystallize the PPDX block until saturation and then quench to suitable temperatures to determine overall isothermal crystallization kinetics. In this case, the nucleation effect of PPDX on PCL can be ascertained and the energy barriers for nucleation and growth determined as a function of composition. Additionally, atomic force microscopy experiments revealed the morphology at the lamellar scale of one selected PPDX-*b*-PCL diblock copolymer during the sequential isothermal crystallization of each block. Finally, preliminary results on hydrolytic degradation are reported.

Experimental

Materials

The controlled synthesis of the well defined PPDX-*b*-PCL diblocks has been described earlier.[44,46] Table 1 denotes the main characteristics of the copolymers such as composition and molecular weight. We employ subscripts to indicate the content of a particular component in weight% and superscripts to indicate the number average molecular weight in kg mol^{-1}.

Polarised optical microscopy (POM)

The polarised optical microscopy experiments were described previously and representative images have been reported.[42,44] The films were prepared by pressing the material between two glass cover slips at 130 °C for 3 min, and then quenched to the desired crystallisation temperature in a Linkam TP-91 hot stage. The samples were observed in a Zeiss MC-80 optical microscope, equipped with crossed polars and a digital camera. Typical errors in the measurement of spherulite growth rates are in the order of 5% or less.

Atomic force microscopy (AFM)

A Veeco Dimension D3100 was used in Tapping Mode using standard silicon cantilevers with a nominal spring constant of 50 Nm^{-1} and a resonant frequency of approximately 250 kHz. The temperature of the sample was controlled using a Linkam heater, using the same experimental set-up as described previously[48] but without the heat-shield as the temperatures required were relatively low. In the phase images shown, soft/sticky areas appear dark and hard materials appear light. Images were collected continuously, each image being collected in approximately 30 s. To allow these high scan rates to be obtained, an ActivResonance Controller from Infinitesima Ltd was used to electronically reduce the effective quality factor of the cantilever from its natural value of around 300 to around 100, giving it a shorter response time and thus allowing faster imaging. The imaging force was adjusted to the minimum that allowed the surface to be successfully tracked by the AFM probe.

Table 1 Molecular characteristics of the materials employed and calorimetric data determined by DSC

				PCL segment						PPDX segment					
				Cooling (10 °C min^{-1})		Heating (10 °C min^{-1})									
Sample	F_{PCL}	M_n^{PCL}/g mol^{-1} [a]	M_n^{PPDX} /g mol^{-1}	T_c/°C	ΔH_c/J g^{-1}	T_{mo}/°C	T_{mp}/°C	ΔH_m/J g^{-1}	χ_c (%)	T_c/°C	ΔH_c/J g^{-1}	T_{mo}/°C	T_{mp}/°C	ΔH_m/J g^{-1}	χ_c (%)
$D_{23}^{8}C_{77}^{27}$	0.77	7510	27 190[b]	31.3	−61.2	54.3	58.2	54.5	50.8	75.4	−1.8	88.3	96.7	14.1	43.4
$D_{40}^{5}C_{60}^{7}$	0.40	7100	4750[b]	30.5	−62.8	55.0	57.0	46.2	55.0	79.2	−1.3	93.7	99.2	34.2	61.0
$D_{65}^{26}C_{35}^{15}$	0.35	15 320	26 200[b]	29.1	−58.3	54.1	56.4	27.0	55.2	77.7	−4.8	93.7	103.9	45.9	50.0
$D_{77}^{32}C_{23}^{10}$	0.23	10 280	32 280[b]	26.3	−52.6	53.0	55.2	17.1	53.2	77.9	−5.8	84.8	104.5	54.1	49.8
PCL[11]	1.00	11 360	—	34.1	−73.1	54.7	56.7	71.9	52.0	—	—	—	—	—	—
PPDX[15]	0.00	—	15 190[c]	52.1	−65.9	—	—	—	—	87.0	−12.1	101.4	107.4	81.0	57.4

[a] Molecular weight of PCL macroinitiator was characterised by GPC in THF at 35 °C.[45] [b] M_n in the copolymers were determined by ^{1}H NMR comparing the relative intensity of both CL and PDX repeating units and knowing M_n of the PCL block.[45] [c] Average molecular weight determined by capillary viscometry (M_v) determined in phenol/1,1,2,2 tetrachloroethane (2 : 3 in vol.) at 25 °C.[2,51] T_{mo} and T_{mp} stand for onset and peak melting temperatures.

Differential scanning calorimetry (DSC)

Aluminium pans were used to encapsulate 5 mg of each sample. A Perkin-Elmer DSC-7 calibrated with indium and hexatricontane standards was employed; all measurements were performed with an ultra high purity nitrogen atmosphere.

Standard DSC experiments

The samples were first heated to 130 °C for 3 min in order to erase the thermal history. Then DSC cooling scans were recorded from 130 °C to −25 °C at 10 °C min^{-1}, followed immediately by a subsequent heating scan also at 10 °C min^{-1} up to 130 °C.

Self-nucleation experiments

The self-nucleation experiments performed are based on experimental protocol previously reported in detail.[25,49] The procedure is carried out as follows: (1) Erasure of thermal history by heating the samples to 130 °C. (2) Creation of a "standard" thermal history by cooling at 10 °C min^{-1} down to −25 °C. (3) Subsequent heating at 10 °C min^{-1} until a temperature is reached that we shall term T_s (or self-nucleation temperature). (4) Thermal conditioning at T_s for 3 min. Depending on the T_s value the sample will be in one of the three self-nucleation domains. If T_s is too high complete melting will occur and the sample will be in Domain I or "Complete Melting" Domain, at which the nucleation density will be constant. If T_s is high enough to melt almost completely all crystals but low enough to leave self-nuclei that increase the nucleation density of the polymer, then the sample is within Domain II or exclusive "Self-nucleation" Domain. Finally, if T_s is too low as to only partially melt the sample, then the sample will be in Domain III or "Self-nucleation and Annealing" Domain, since the not melted crystals will anneal during the 3 min at T_s. (5) Cooling from T_s at 10 °C min^{-1} during which the effect of self-nucleation will be revealed and (6) final subsequent heating scan, at 10 °C min^{-1}, where the presence or absence of annealing effects will be seen. The DSC scans during steps 5 and 6 are usually presented to examine the effects of the self-nucleation treatment.

Isothermal DSC experiments

Isothermal crystallisation of the PCL and PPDX homopolymers were performed after melting the samples for 3 min at 130 °C and then they were quenched (at 80 °C min^{-1}) to the desired isothermal crystallization temperature or T_c.

Isothermal crystallisation of PCL block

Samples were first melted at 130 °C for 3 min, then they were cooled down to −25 °C at 10 °C min^{-1} to promote the crystallisation of both PPDX and PCL blocks. After that, the samples were heated up to 62 °C, a temperature above the melting temperature of the PCL component. The samples were annealed at this temperature for 70 min to guarantee that PPDX had crystallized until saturation. Finally, the samples were quenched (80 °C min^{-1}) to T_c and the overall isothermal crystallization was monitored by the DSC.

Self-nucleation followed by isothermal crystallization

In some cases, in order to be able to register with the DSC the isothermal crystallization of the PPDX block which proceeded very slowly in some diblock copolymers, the sample was first self-nucleated employing a T_s temperature within Domain II and then it was quenched (80 °C min^{-1}) to T_c. Experiments were performed to check that the sample did not crystallize during the cooling to T_c and that a full crystallization exotherm was recorded at T_c.

Hydrolytic degradation experiments

The $PPDX^{15}$, $D_{65}^{26}C_{35}^{15}$ and $D_{77}^{32}C_{23}^{10}$ were hydrolytically degraded in a 0.2 M (pH 7.4) phosphate buffered saline solution at 37.2 ± 0.2 °C for 9 months. The buffers were replaced every 10 days, in order to maintain a constant pH during the whole degradation process. The samples were extracted monthly, dried at 25 °C under vacuum for 48 h, and then weighted. The compositions of the diblock copolymers were recalculated after hydrolysis by ^{1}H NMR spectroscopy knowing the relative intensities of methylene protons of the PDX repeat units at 4.38 ppm and methylene protons of CL repeat units at 2.32 ppm, using a Bruker AMX-300 apparatus in d^2-1,1,2,2-tetrachloroethane/TMS.[42,46]

Results and discussion

General thermal behaviour

Fig. 1 presents DSC cooling and subsequent heating scans for the PPDX-*b*-PCL diblock copolymers in a wide composition range, for comparable molecular weight homopolymers and for a 50/50 PPDX/PCL blend. The cooling scans indicate that regardless of the composition in the diblock copolymers only one crystallization exotherm is observed. In a previous work[42] this behaviour was examined by time resolved WAXS and isothermal crystallization kinetics and it was concluded that a coincident crystallization process takes place.

During cooling at 10 °C min^{-1} the PPDX block cannot crystallize at the same temperature as the equivalent homopolymer because its secondary nucleation is hindered by the covalently bonded molten PCL block, therefore it needs a larger undercooling to start its crystallization. New evidence that supports this explanation will also be presented in the present work. Once the crystallization of the PPDX block starts, it is quickly followed by the crystallization of the PCL block which can be nucleated by the PPDX block. As a result, the crystallization of both blocks occurs in the same temperature range and in a quick succession leading to an overlap of the DSC exothermic signal during cooling. This overlap can not be overcome by the use of slower cooling rates, at least down

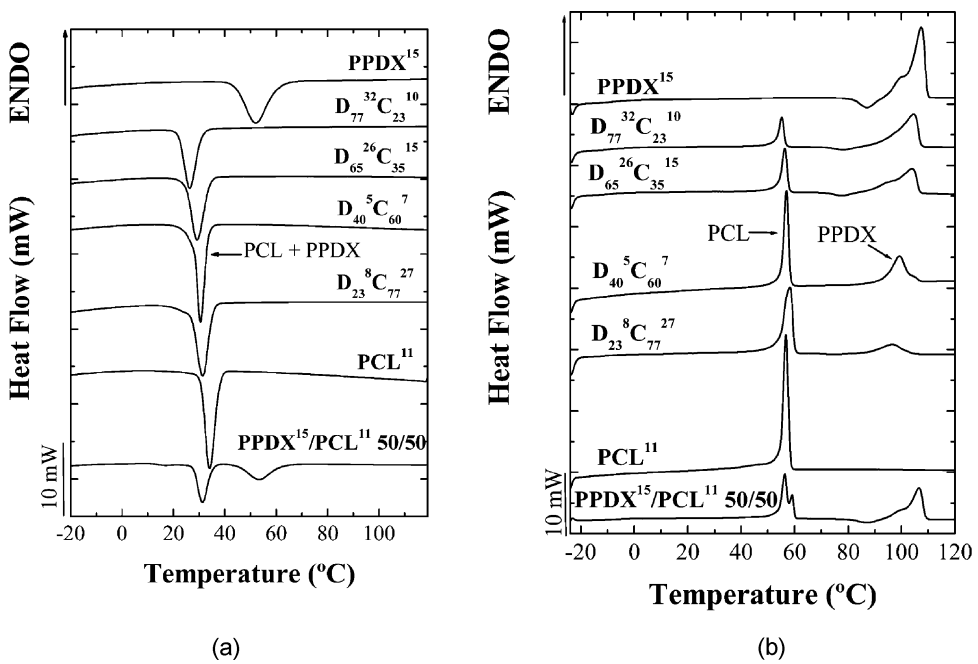

Fig. 1 (a) DSC cooling scans (10 °C min^{-1}) for PCL and PPDX homopolymers, diblock copolymers and a 50/50 blend. (b) Subsequent heating scans (10 °C min^{-1}).

to 1 °C min^{-1}. This may be related to the fact that the PCL only crystallizes after the PPDX block starts to crystallize, this was clearly demonstrated by previous WAXS results.[42]

In a related double crystalline polyethylene-*b*-poly(L-lactide) diblock copolymer (with an approximate 50/50 weight ratio) a similar behaviour has been observed.[50] When the diblock copolymer is cooled from the melt at 10 °C min^{-1} only one crystallization exotherm is observed indicating that the L-lactide block is also being affected by the molten polyethylene block that is covalently bonded to it.[50] However in this case, the crystallization exotherms can be separated by reducing the cooling rate to 2 °C min^{-1}.[41]

The data shown in Fig. 1(a) for a 50/50 blend supports the above explanation since the individual crystallization of each blend component can clearly be observed. It will also be demonstrated below that when self-nucleation is applied, the crystallization signals of each block can be separated.

The DSC heating scans in Fig. 1(b) show that each phase melts in a very different temperature range and that the melting temperatures are close to those exhibited by the equivalent homopolymers (see Table 1). The ability of PPDX to reorganize during heating has been reported previously[51] and a cold crystallization exotherm can be seen in some of the heating DSC scans in Fig. 1(b).

Table 1 indicates that the melting point of the PPDX block reduces as its content within the copolymer is decreased, while the melting point of the PCL block remains constant. Table 1 also reports the enthalpy of fusion of each constituent and the degree of crystallinity calculated with those values once they have been normalized by the composition, no clear trend is observed as a function of composition.

Morphology

The observation of the MD morphology in PPDX-*b*-PCL diblock copolymers has been challenging. PPDX and PCL are apparently not miscible in spite of their chemical similarities.[42] We have prepared a series of PPDX and PCL blends employing polymers in a wide range of molecular weights and none of the blends have shown signs of miscibility. The lower limit in M_n explored so far was a blend of 5000 g mol^{-1} PPDX with a PCL of just 600 g mol^{-1}. In this case, as in all others, pieces of evidence of immiscibility were obtained: (a) the blend exhibited two glass transition temperatures at values close to those corresponding to the homopolymers; (b) there was no significant melting point depression for the PPDX block (or any change in the melting point of the PCL block) regardless of the PCL content in the blend and (c) a two phase morphology was observed in scanning electron microscopy experiments.

In view of the above, and of rather similar results obtained with our diblock copolymers (similar trends regarding T_g and T_m values being independent of composition and similar to values exhibited by homopolymers of equivalent molecular weights), we have considered that the PPDX-*b*-PCL diblock copolymers should exhibit phase segregation in the melt. If they are phase segregated in the melt they must be in the weak segregation limit considering their molecular structures and solubility parameters.[42] However, we have not been able to obtain so far any direct evidence of the MD structure in the melt. The order–disorder transition has not been directly detected since decomposition of the PPDX at temperatures higher than 140 °C mask thermal events at such higher temperatures.[42] Since PPDX has a higher susceptibility to both hydrolytic degradation and thermal degradation than PCL,[1,2] we have not been able to anneal the samples in the melt for a long time in order to perfect the possible heterogeneous melt morphology. As a consequence of this, previous attempts to measure SAXS have resulted in broad scattering peaks with no higher order reflections indicating the absence of long range order,[42] this may also indicate that the melt is homogeneous. So far, staining attempts with several agents have failed to reveal the morphology by TEM, although work in still in progress in this respect.

If we refer to the introduction, we have previously[42] made the reasonable assumption that PPDX-*b*-PCL copolymers fall within case number 2, *i.e.*, a weakly segregated system with soft confinement for the PPDX block, since it crystallizes first, so that $T_{ODT} > T_c > T_g$. It should be noted that if crystallization proceeds from a homogeneous melt (case 1) or from a weakly segregated melt with soft confinement (case 2), the crystallization should occur in both cases with a lamellar morphology (which either comes from a homogeneous melt or from a "break-out" morphology that overwrites the MD morphology present in the melt[17]).

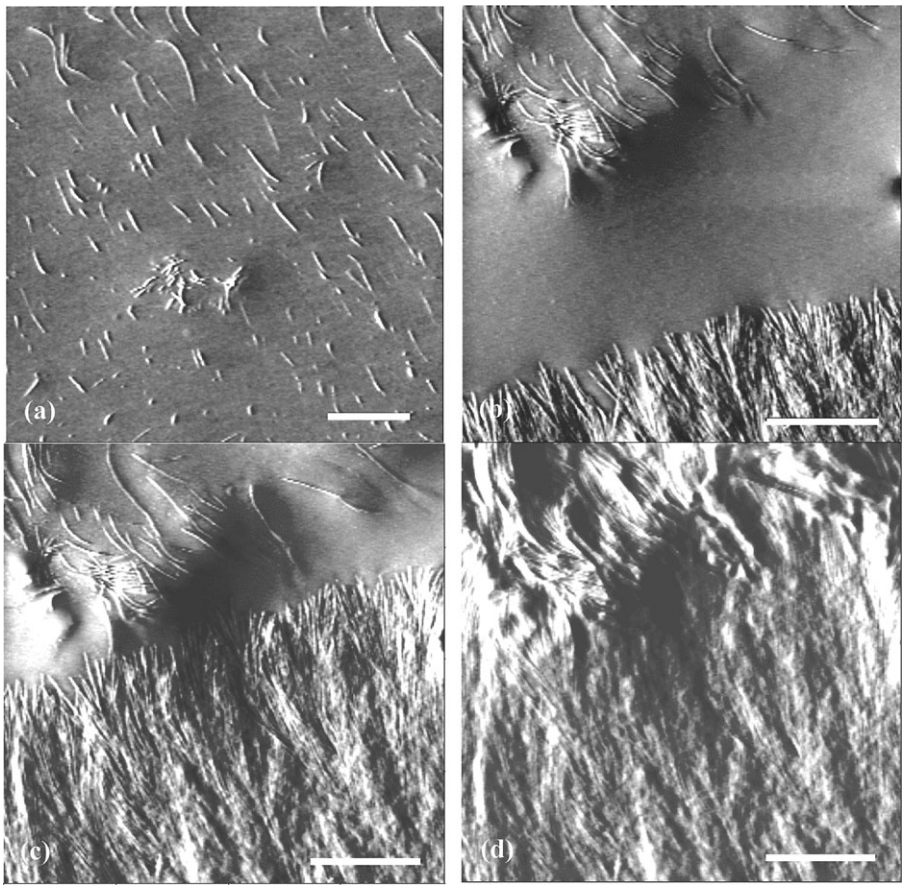

Fig. 2 A series of AFM images taken during sequential isothermal crystallization of $D_{23}^{8}C_{77}^{27}$. (a) The sample was isothermally crystallized at 60 °C, only PPDX can crystallize at this temperature. (b) Through (d), the sample was quenched to 40 °C and images are taken at increasing times: (b) $t_b = t$, (c) $t_c = t + 2$ min, (d) $t_d = t + 5.5$ min. Scale bars represent 1 μm.

Previous reports[42,44] dealing with PPDX-*b*-PCL diblock copolymers have shown by POM that superstructural aggregates with a predominant granular texture are obtained at temperatures around 50 °C or higher (at such high T_c values only the PPDX block is able to crystallize and in copolymers with a higher content of PPDX the Maltese cross extinction pattern was observed in a clearer spherulitic texture) while banded spherulites composed of both blocks are present at lower temperatures.

Recently, we have been able to perform AFM observations in $D_{23}^{8}C_{77}^{27}$. The observations in the melt indicated a grainy appearance and it was difficult to ascertain whether a MD melt morphology was present or not. For this sample, and based on the composition, a PCL matrix with PPDX spheres or cylinders should be expected, if the melt were heterogeneous.

Fig. 2(a) shows the morphology obtained after lowering the temperature to 60 °C, a temperature too high for the PCL block to crystallize (peak T_m value for the PCL block was 58 °C, see Table 1). PPDX lamellae can be seen in Fig. 2(a) in a molten PCL matrix. They seem to be approximately randomly distributed although some connections between lamellae can be observed as well as some lamellar aggregates. The fact that lamellae are present may be an indication that some form of "breakout"[17] has been generated during crystallization facilitated by the soft confinement or that crystallization from a homogeneous melt is in place and PPDX lamellae are being formed. In any case, it is clear that crystallization is driving structure formation.

The temperature was then lowered to 40 °C, a temperature at which the PCL block can now crystallize isothermally. Fig. 2b shows in the top part previously crystallized PPDX lamellae (at 60 °C) and in the bottom part newly formed PCL lamellae that belong to a growing spherulite (PCL amounts to 77% for this copolymer). In the sequence of micrographs shown in Figs. 2(b)–(d) the spherulite can be seen as it grows past the previously crystallized PPDX lamellae and these are engulfed by the growing superstructure. A mixed spherulite containing lamellae of both PPDX and PCL results and can be observed in Fig. 2(d). See also a video in the ESI showing the sequential isothermal crystallization of $D^{8}_{23}C^{27}_{77}$ according to the same temperature program described in Fig. 2.†

Crystallization kinetics from growth rate data

We have followed by POM the radial growth of spherulites at temperatures where only the PPDX can crystallize for a $D^{32}_{77}C^{10}_{23}$ diblock copolymer and PPDX[15] homopolymer. This diblock copolymer showed clearly spherulitic features with Maltese cross when crystallized at temperatures where the PCL was molten. Fig. 3(a) shows the experimentally determined spherulitic growth rates (G) as a function of crystallization temperature. The difference in growth rates is very pronounced between the homopolymer and the PPDX block within the diblock copolymer and amounts to an order of magnitude at certain crystallization temperatures. This difference demonstrates that the PPDX block is experiencing secondary nucleation problems because it is covalently bonded with the molten and highly flexible PCL. This indicates that the coincident crystallization phenomenon observed in Fig. 1 is caused not only by a reduction in nucleation that the PPDX block may be experiencing as compared to PPDX homopolymer.

We have applied the Lauritzen and Hoffman kinetic treatment to the growth rate data by considering that G can be expressed as:[52,53]

$$G(T) = G_0 \exp\left(-\frac{U*}{R(T_c - T_\alpha)}\right) \exp\left(-\frac{K_g^G}{T\Delta T f}\right) \quad (1)$$

where G_0 is a growth rate constant, U* is the activation energy for the transport of the chains to the growing nuclei, a value of 1500 cal mol^{-1} is normally employed,[53] R is the gas constant and T_c the isothermal crystallization temperature. T_α is a temperature at which chain mobility ceases and it is usually taken as T_g-30 (K),[53] however, we found a better fit to our data with a value of T_g-15 (K). ΔT is the supercooling defined as $(T_m^\circ - T_c)$, where T_m° is the equilibrium melting point. The factor f is a temperature correction term equal to: $2T_c/(T_c + T_m^\circ)$.[52,53] Finally, K_g^G is an important

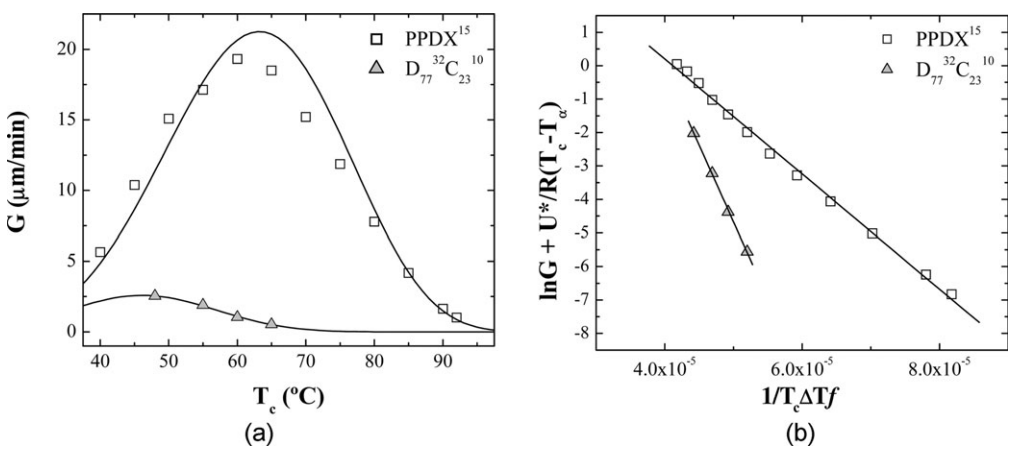

Fig. 3 (a) Spherulitic growth rates for PPDX and the PPDX block within $D^{32}_{77}C^{10}_{23}$ diblock copolymer. Solid lines are fits to the Lauritzen and Hoffman theory according to eqn. (1). (b) Lauritzen and Hoffman kinetic theory plot for PPDX and the PPDX block within $D^{32}_{77}C^{10}_{23}$ diblock copolymer.

parameter since it can be considered proportional to the energy barrier for secondary nucleation or growth and is given by:[52,53]

$$K_g^G = \frac{jb_0\sigma\sigma_e T_m^0}{k\Delta h_f} \quad (2)$$

where j is taken as 2 for Regime II, b_0 is the width of the chain, σ is the lateral surface free energy, σ_e is the fold surface free energy, k is the Boltzmann constant and Δh_f the heat of fusion of a perfect crystal.

Fig. 3(b) shows the usual way of fitting the experimental data to the theory by plotting $\ln G + U/R(T_c - T_\alpha)$ *versus* $1/(T_c\Delta Tf)$, a straight line should be obtained and K_g^G can be determined from the slope of the plot. We have assumed that crystal growth occurs under Regime II and the values of all parameters employed for the calculation are listed in Table 2. Once we determined K_g^G, we calculated the theoretical prediction from eqn. (1) and plotted the results over the experimental data points in Fig. 3a, the use of a linear scale highlights the differences between experiment and theory which are masked in Fig. 3b by the use of logarithms and reduced parameters.

A typical bell shape curve in the spherulitic growth kinetics of PPDX (Fig. 3a) has been obtained.[54] Previously, we had only been able to access (with different molecular weight PPDX samples) the nucleation controlled right hand side of the curve.[2,51] Other authors[55] have obtained similar bell shape curves from overall PPDX homopolymer crystallization rate data.

Table 2 shows the values obtained for K_g^G for PPDX[15] and the PPDX block within $D_{77}^{32}C_{23}^{10}$. It can be observed that the K_g^G value for the PPDX block within the copolymer is more than twice that of neat PPDX[15]. This gives an idea of the difficulty that this block encounters to crystallize with a covalent PCL chain attached to it as compared to neat PPDX.

From the values of K_g^G the product $\sigma\sigma_e$ is obtained according to eqn. (2). The following expressions allow the calculation of σ (and therefore σ_e) and q, the work done by the chain to form a fold:

$$\sigma = 0.1\Delta h_f\sqrt{a_0 b_0} \quad (3)$$

$$q = 2a_0 b_0 \sigma_e \quad (4)$$

where $a_0 b_0$ is the cross sectional area of the chain. As expected from the K_g^G values, both the fold surface free energy and the work for chain folding are much higher for the PPDX block within $D_{77}^{32}C_{23}^{10}$ than for the PPDX[15] homopolymer, as shown in Table 2. The range of values obtained for the fold surface free energies are consistent with previous literature reports for PPDX, PCL and polyesters in general.[2,51,53]

In this section we have shown that the energy barrier for growing spherulitic superstructures is higher for a PPDX block within $D_{77}^{32}C_{23}^{10}$ than for the PPDX[15] homopolymer. This supports previous evidence[42,44] suggesting that the molten PCL block covalently bonded to the crystallizing PPDX block is hindering the secondary nucleation process. More new evidence in this respect is presented below.

The dramatic depression of the growth rate in the PPDX block within the $D_{77}^{32}C_{23}^{10}$ diblock copolymer as compared to an equivalent molecular weight homopolymer is the determining factor in the coincident crystallization behaviour encountered upon cooling the copolymer from the melt in Fig. 1.

Overall crystallization kinetics for the PCL block within PPDX-*b*-PCL diblock copolymers

In a previous work,[42] it was demonstrated that if both blocks are simultaneously crystallized by quenching the diblock copolymer from the melt directly to a low crystallization temperature, a slower kinetics is observed than when the PPDX block is allowed to crystallize at high T_c and then the sample is quenched to a lower crystallization temperature and the PCL block is crystallized. Therefore a nucleating effect of the PPDX on the PCL was proposed to explain this behaviour.

The PPDX block was first crystallized until saturation and then the temperature was lowered to the crystallization temperature of the PCL block (see experimental). The quality of the data obtained can be appreciated in Fig. 4, where examples of isothermal DSC scans for the

Table 2 Values obtained by fitting the Lauritzen and Hoffman theory to experimental data and parameters employed in eqn. (1)–(4) and (6)

Sample	T_c range/°C	T_α/K	$K_g^G \times 10^{-4}$/K^2	$K_g^\tau \times 10^{-4}$/K^2	σ_e^G/erg cm^{-2}	σ_e^τ/erg cm^{-2}	$q^G \times 10^{-13}$/erg	$q^\tau \times 10^{-13}$/erg	σ/erg cm^{-2}
PCL[11]	40–50	192.7	7.0 ± 0.1	10.0	80.1	113.6	3.0	4.2	7.0
$D_{23}^{8}C_{77}^{27}$	40–50	192.7		9.6		108.8		4.0	7.0
$D_{40}^{5}C_{60}^{7}$	40–50	192.7		12.6		143.6		5.3	7.0
$D_{65}^{26}C_{35}^{15}$	40–44	192.7		12.7		144.6		5.3	7.0
$D_{77}^{32}C_{23}^{10}$	44–46	192.7		16.3		185.6		6.8	7.0
PPDX[15]	40–90	248.2	17.2 ± 0.4	31.0	168.1	302.6	6.2	11.2	8.1
$D_{77}^{32}C_{23}^{10}$	48–65	248.2	46 ± 2		448.0		16.5		8.1
PPDX[15] sn 117 °C	85–95	248.2		17.0		166.3		6.1	8.1
$D_{77}^{32}C_{23}^{10}$ sn 110 °C	60–70	248.2		31.0		303.4		11.2	8.1
$D_{65}^{26}C_{35}^{15}$ sn 110 °C	55–65	248.2		42.7		417.6		15.4	8.1

Values for eqn. (1) and (3) include: $a_o = 4.5$ Å, $b_o = 4.1$ Å and $U^* = 1500$ cal mol^{-1} which correspond to PCL and were employed for all materials.[51,53] For PCL and PCL blocks the value of T_m° employed was 70.9 °C (literature values range from 70.3–74 °C[53]) and for PPDX and PPDX blocks T_m° was taken as 127.1 °C.[51] Superscripts G and τ are used to indicate that a value was calculated from spherulitic growth rate data (G) or from DSC overall crystallization rate data ($1/\tau_{50\%}$) respectively. Values of ΔH_f for PPDX and PCL were taken as: 141.2 J g^{-1} and 139.5 J g^{-1} respectively.[2,51,63] The unit cell densities used were 1.175 g cm^{-13}, for the PCL and PCL block, and 1.332 g cm^{-13} for the PPDX and PPDX block, respectively.[63] Errors in K_g^τ are estimated to be less than 2.5%. sn: self-nucleated material at the indicated T_s temperature, see text.

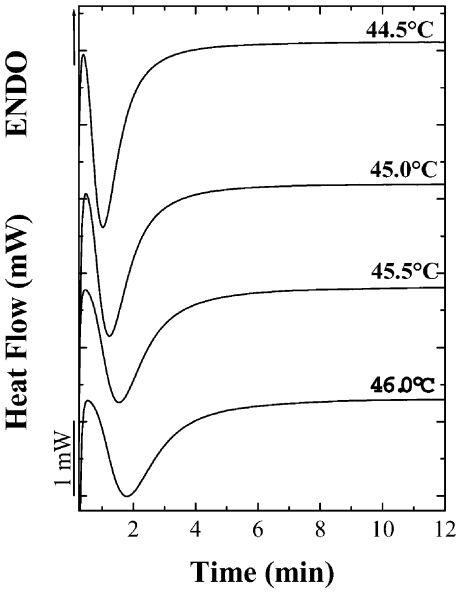

Fig. 4 Examples of DSC isothermal crystallization scans for the PCL block within $D_{40}^{5}C_{60}^{7}$ diblock copolymer. The measurements are performed after the PPDX block had been previously crystallized until saturation (see experimental).

crystallization of the PCL block are presented. The data obtained has been initially analysed with the Avrami equation:[53,54,56]

$$X(t) = 1 - \exp(-Kt^n) \tag{5}$$

where $X(t)$ is the relative crystalline volume fraction of the polymer as a function of time. The parameters K and n are dependent on the nucleation type and the crystal growth geometry, K can be considered an overall transformation rate constant and n is the Avrami index.

The overall crystallization rate, expressed as the inverse of the experimental crystallization half-time, for PCL[11] and for the PCL block of the diblock copolymers employed in this work are shown in Fig. 5, where the nucleation effect of the previously crystallized PPDX block on the PCL block is confirmed. The overall crystallization rate of the PCL block in the case of $D_{23}^{8}C_{77}^{27}$ and $D_{40}^{5}C_{60}^{7}$ is higher than that of PCL[11]. This effect was reported in a previous work when the PPDX content in the copolymer was lower than 53%.[44] In cases where the PPDX content in the diblock copolymer was equal or more than 53%, the nucleation effect of the PPDX block on the PCL seems to be overtaken by topological restrictions. Fig. 5 shows that the PCL blocks within $D_{77}^{32}C_{23}^{10}$ and $D_{65}^{26}C_{35}^{15}$ crystallize at a slower overall rate than neat PCL. In these cases, the PPDX matrix has already crystallized in spherulites and the 23% or 35% PCL must crystallize within them. Interestingly, we have found no fractionated crystallization effects during cooling from the melt in Fig. 1 for $D_{77}^{32}C_{23}^{10}$ or $D_{65}^{26}C_{35}^{15}$, which can be explained by the nucleating influence of the PPDX block. In fact, Fig. 5 demonstrates that even under isothermal conditions the PCL block in these copolymers can crystallize in a similar temperature range to the PCL homopolymer, a clear indication of a heterogeneous nucleation mechanism.[25]

Even though the nucleating effect of the PPDX on the PCL prevents any homogeneous nucleation, increasing amounts of PPDX within the PPDX-*b*-PCL diblock copolymers hinders crystallization of the PCL block as already indicated above by an overall reduction in kinetics (Fig. 5). Fig. 6 shows how the Avrami index depends on the PCL content in the diblock copolymers for a wide temperature range. In this plot we have collected all the data from previous works[42,44] as well as recent data. The Avrami index is found to decrease as the PCL content in the copolymer decreases. Such a decrease in Avrami index can be interpreted as a decrease in the dimensionality of growth of the PCL block superstructures as more previously crystallized PPDX is present in the sample.

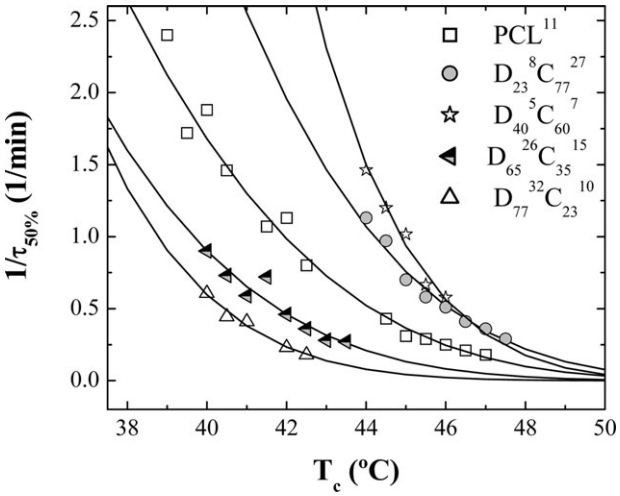

Fig. 5 Inverse of the crystallization half-time as a function of isothermal crystallization temperature for PCL[11] homopolymer and for the PCL block of the indicated copolymers. All experiments were performed after the PPDX block had been previously crystallized until saturation (see experimental). Solid lines are fits to the Lauritzen and Hoffman theory according to eqn. (6).

It is well known that when a polymer is confined into a great number of isolated MD (*e.g.*, spheres or cylinders) it crystallizes from homogeneous nuclei that form at the largest possible supercooling.[25] When such a situation arises, Loo *et al.*[38] have shown that the Avrami index is usually 1.

For the $D_{77}^{32}C_{23}^{10}$ case, where the highest possible confinement of the PCL block would be expected, the Avrami index was found to be larger than 1, a result which confirms the absence of homogeneous nucleation. The Avrami index obtained for this copolymer was of the order of 2 and could correspond to one-dimensional crystals grown from sporadic nuclei, or two-dimensional growth from instantaneous nuclei. If the PCL phase is not isolated in a large number of MD but connected throughout by percolation paths, this allows the spread of secondary nucleation and an

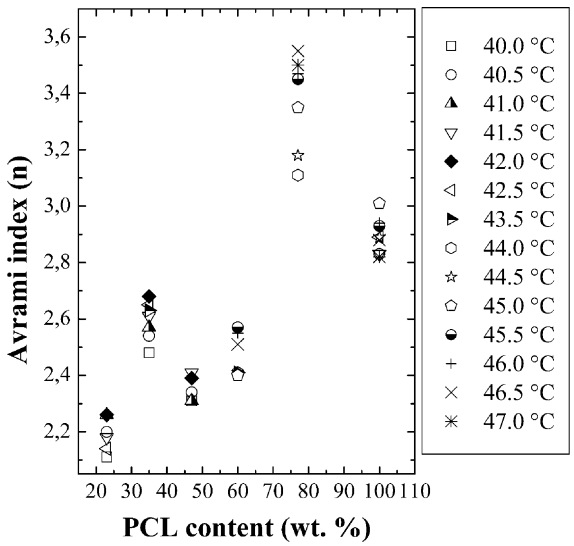

Fig. 6 Variation of the Avrami index with PCL content in PPDX-*b*-PCL diblock copolymers at the indicated crystallization temperatures.

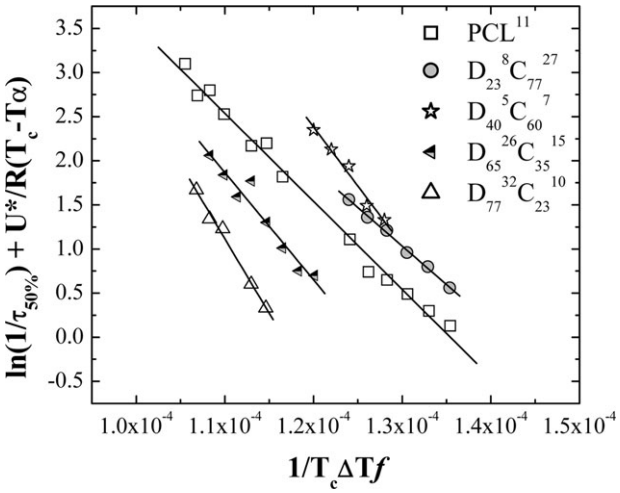

Fig. 7 Lauritzen and Hoffman kinetic theory plots for PCL[11] homopolymer and for the PCL block of the indicated copolymers. All experiments were performed after the PPDX block had been previously crystallized until saturation (see experimental).

Avrami index larger than 1 would also be obtained. Nevertheless, many features are consistent with a nucleation effect of the PPDX crystals on the PCL phase (and more will be given below, see Fig. 9) that this must be the dominant factor, although interconnection of MD could also be present.

As the PCL content in the copolymer increases the Avrami index increases to values that are similar to those of PCL homopolymer, *i.e.*, around 3, indicating spherulitic growth that has been confirmed by POM observations.[42]

The temperature dependence of the inverse of the half-crystallization time can be assumed to have a form similar to eqn. (1):[54,57,58]

$$\frac{1}{\tau_{50\%}}(T) = G_o^{\tau} \exp\left(-\frac{U^*}{R(T_c - T_\infty)}\right) \exp\left(-\frac{K_g^{\tau}}{T\Delta T f}\right) \tag{6}$$

where $\tau_{50\%}$ is the overall crystallization half-time determined from DSC measurements. The inverse of $\tau_{50\%}$ represents a measure of the overall crystallization rate that takes into account both nucleation and growth. The pre-exponential factor and the term K_g in eqn. (6) have a τ superscript to indicate that they are both now a function of nucleation and growth.

Fig. 7 shows a plot of $\ln(1/\tau_{50\%}) + U^*/R(T_c - T_\infty)$ *versus* $1/(T_c \Delta T f)$ according to eqn. (6) for PCL[11] and for the PCL block within four different diblock copolymers. It can be seen that in all cases good fits to straight lines allow the determination of K_g^{τ}. The values obtained are reported in Table 2 and were employed to fit the experimental data of Fig. 5 with eqn. (6), the quality of the fit can be appreciated in a linear scale in this case, all fits were excellent.

It is interesting to see how the value of K_g^G compares with K_g^{τ} in the case of the PCL[11] homopolymer reported in Table 2. K_g^{τ} is larger than K_g^G by 30% indicating that the process of nucleation and growth has a larger energetic barrier than the process of spherulite growth only. The fact that the K_g^{τ} value of the PCL block within $D_{23}^{8}C_{77}^{27}$ is almost the same as that of PCL[11] homopolymer may indicate that the nucleating effect of the PPDX block is already counter balanced by the presence of the PPDX crystals, since a value of the order of K_g^G (*i.e.*, $7.0 \pm 0.1 \times 10^4$ K^2, see Table 2) would be expected if 100% nucleation efficiency of the PPDX is assumed.

Table 2 shows that the values of K_g^{τ} for the PCL block within the copolymers increase as the content of PPDX in the copolymer increases, indicating the difficulty encountered by the PCL chains to crystallize as more crystalline PPDX material is present in the copolymer. As a result of the increase in K_g^{τ} the values for the fold surface free energy and the work to fold the PCL chains also increase as the content of PCL within the copolymers decreases.

We tried to follow the same procedure employed to determine the overall crystallization kinetics of the PCL block within the PPDX-*b*-PCL diblock copolymers in POM experiments but once the PPDX was crystallized the nucleation density was so high that the PCL spherulites were very small and their growth could not be followed by POM.

Self-nucleation studies

The technique of self-nucleation was applied initially to PPDX and PCL and later to the PPDX-*b*-PCL diblock copolymers. In the case of PPDX[15], Fig. 8(a) shows DSC cooling scans from selected self-nucleation temperatures, T_s, and Fig. 8(b) the corresponding subsequent heating scans after self-nucleation at T_s.

If the T_s temperature is equal or higher than 125 °C the melting is complete and no new nuclei are generated after 3 min at such temperatures. Therefore the sample is considered to be under Domain I or complete melting Domain and its crystallization temperature during cooling from T_s does not change since it reflects a constant nucleation density.

When the T_s temperature is lower than 125 °C, the crystallization temperature increases because self-nuclei have been generated by the thermal treatment at T_s, and the samples are in Domain II. The high temperature melting peak does not show any signs of annealing until the T_s temperature is lowered into Domain III. The low temperature shoulder does change with T_s temperature within Domain II. These changes are related with the increased crystallization ability of PPDX once it has been self-nucleated in Domain II and how this reflects in its reorganization capacity during the subsequent heating scan, the reader is referred to ref. 51 for more details.

Finally, if the T_s temperature is too low, partial melting and annealing occurs together with self-nucleation. The annealing can be seen in the subsequent heating runs, like that shown in Fig. 8(b) for $T_s = 105$ °C, indicated by an arrow. The self-nucleation behaviour of PPDX[15] is the standard general behaviour of semi-crystalline homopolymers.[49] A similar standard behaviour was obtained for the PCL[11] homopolymer (results not shown).

It is interesting to examine the self-nucleation behavior of the diblock copolymers for two reasons. First, to try to separate by temperature the coincident crystallization shown in Fig. 1 by

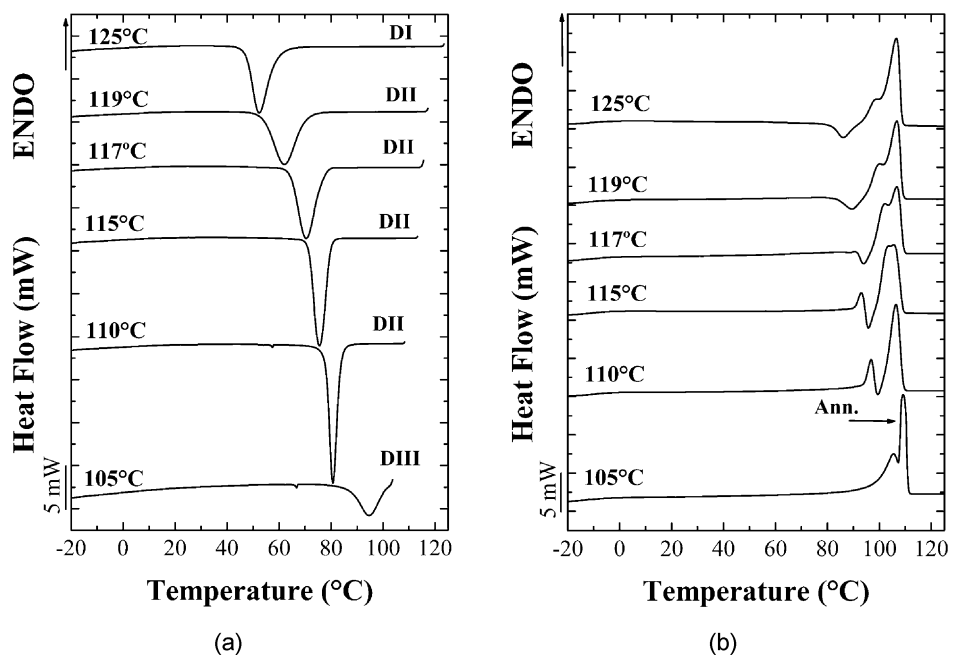

Fig. 8 Self-nucleation of PPDX[15]: (a) DSC cooling scans from the indicated T_s temperatures; (b) subsequent heating scans.

self-nucleating just the PPDX block, and second, because it has been shown in a wide range of crystallizable diblock and triblock copolymers that if a particular phase is isolated and crystallizes in a large number of individual microdomains (like spheres or cylinders for instance) Domain II usually disappears and a direct transition from Domain I to Domain III has been observed.[25,59–61]

Fig. 9(a) presents self-nucleation results for $D_{77}^{32}C_{23}^{10}$ in a T_s temperature range where self-nucleation affects only the PPDX block. At $T_s = 115\,^{\circ}C$ the sample is in Domain I and the coincident crystallization of both blocks occurs with a single exotherm that peaks at around 26 °C. At $T_s = 110\,^{\circ}C$ the sample is under Domain II and self-nucleation occurs as indicated by the higher peak crystallization temperature of the coincident main exotherm. Close observation of that cooling DSC scan reveals a downwards drift of the baseline upon cooling from approximately 60 °C that indicates that some PPDX crystals are crystallizing at higher temperatures, in Fig. 9(a) a close up of a section of this curve highlights this observation. For a $T_s = 108\,^{\circ}C$ it is very clear that the PPDX has been self-nucleated and is now crystallizing at higher temperatures in a complex bimodal exotherm. A similar behaviour is seen for $T_s = 107\,^{\circ}C$ except that the exotherms corresponding to the PPDX are slightly shifted to higher temperatures. For $T_s = 104\,^{\circ}C$ the crystallization occurs immediately upon cooling, a typical sign that indicates partial melting and annealing.[25,49] In fact the annealing can be observed in the heating scan corresponding to $T_s = 104\,^{\circ}C$, where a very sharp high temperature second melting peak is observed and indicated by an arrow (Fig. 9(b)).

Another interesting point from the self-nucleation results reported in Fig. 9a is the fact that at rather low T_s temperatures within Domain II, *e.g.*, at $T_s = 107\,^{\circ}C$, or even within Domain III, *i.e.*, $T_s = 104\,^{\circ}C$, most of the PPDX that was going to be self-nucleated by the treatment is crystallizing at much higher temperatures than the PCL block (an estimate of the amount of PPDX that has been self-nucleated, based on the differences between the crystallization and fusion enthalpies is given in Fig. 9a for two T_s temperatures). Therefore, the remaining exotherm located at around 30 °C must correspond mainly to the crystallization of the PCL block and its crystallization temperature is also shifted to higher temperatures as compared to the standard sample (*i.e.*, that with $T_s = 115\,^{\circ}C$). Therefore, this result also indicates that the PPDX block can nucleate the PCL block and it seems

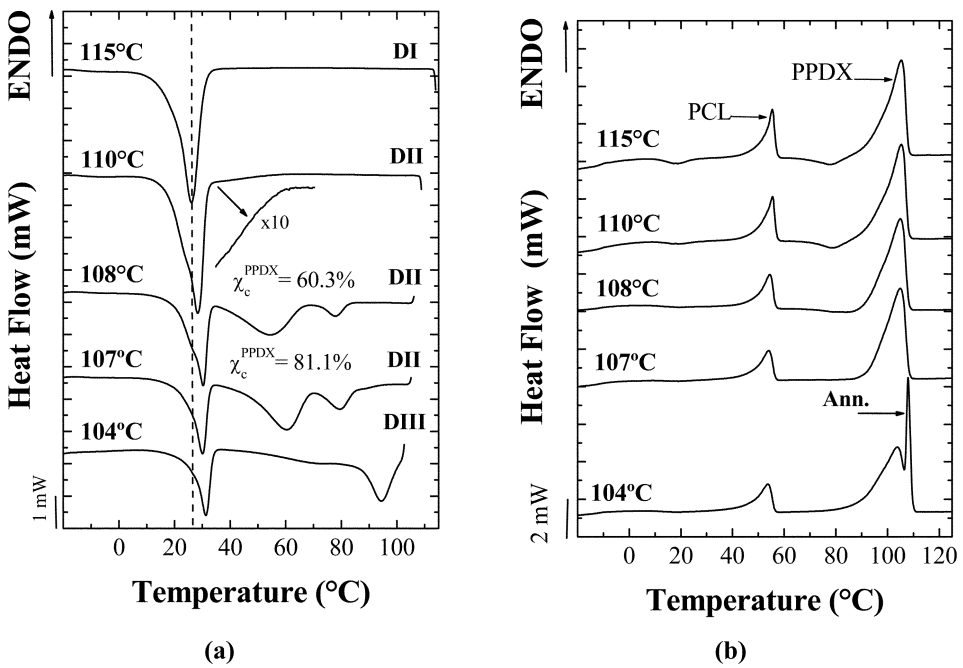

Fig. 9 Self-nucleation of the PPDX block within $D_{77}^{32}C_{23}^{10}$: (a) DSC cooling scans from the indicated T_s temperatures. χ_c^{PPDX} represents the amount of PPDX that has been self-nucleated; (b) Subsequent heating scans. The arrow points to the melting endotherm of annealed crystals during treatment at T_s.

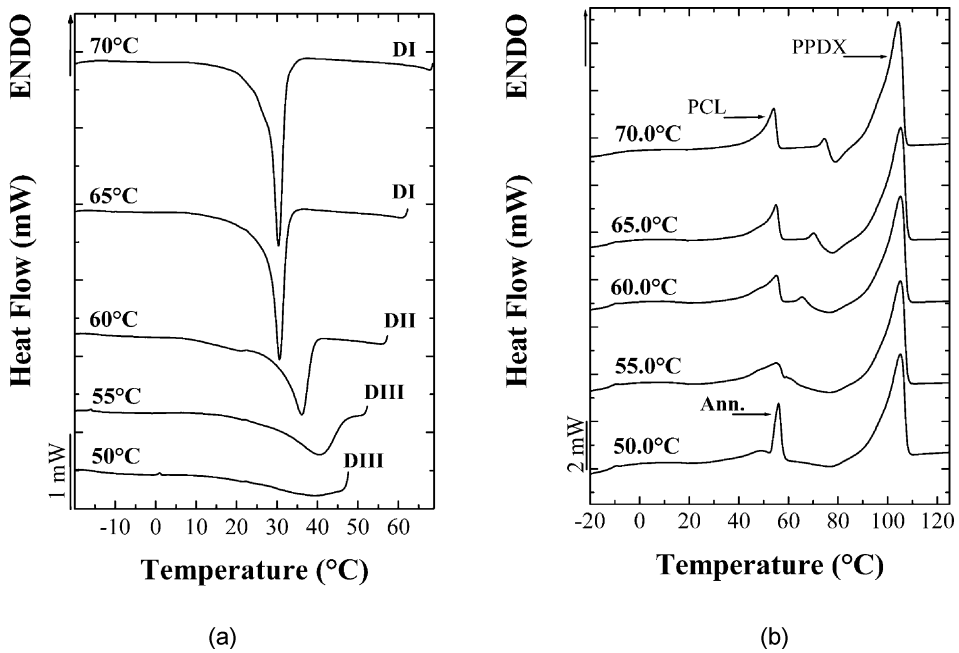

Fig. 10 Self-nucleation of the PCL block within $D_{77}^{32}C_{23}^{10}$: (a) DSC cooling scans from the indicated T_s temperatures; (b) subsequent heating scans. The arrow points to the melting endotherm of annealed crystals during treatment at T_s.

the effect is more pronounced when the PPDX nucleation density has been greatly increased by the self-nucleation treatment.

Fig. 10a shows cooling scans from T_s for $D_{77}^{32}C_{23}^{10}$ in a temperature range where the PCL block self-nucleation can be studied. Fig. 10(b) presents the subsequent heating scans. The analysis of Fig. 10 indicates that the PCL block can be self-nucleated in a standard way and all three self-nucleation Domains can be clearly identified, and have been labelled in Fig. 10(a). This result has an important implication since it corroborates that in spite of its small amount within the copolymer, the PCL block still shows a clear Domain II and therefore does not show signs of homogeneous nucleation.[25,59–61] Since we have presented evidence which indicates that the previously crystallized PPDX block can nucleate the PCL block, then the lack of homogeneous nucleation or fractionated crystallization can be attributed to a heterogeneous nucleation effect produced by the PPDX crystals on the PCL chains. On the other hand, the existence of a percolation path of the PCL crystals may also contribute to spread nucleation.

Isothermal crystallization after self-nucleation

We tried to measure the overall isothermal crystallization kinetics by DSC for the PPDX block within the PPDX-*b*-PCL diblock copolymers in a temperature range where only the PPDX can crystallize (*i.e.*, at T_c higher than 50 °C). Unfortunately, the overall crystallization rate was so slow that the DSC was not able to measure any significant exothermic signal in the isothermal mode. One way to circumvent this limitation is to self-nucleate the material first and then quench it (at a controlled cooling rate of 80 °C min^{-1}) to its isothermal crystallization temperature. In this way two interesting results could be obtained. Firstly, the acceleration of the overall kinetics provided by the self-nucleation treatment allows the DSC to measure the isothermal crystallization kinetics. Secondly, the measured kinetics should be closer to that obtained by POM because they should reflect mostly the growth of the crystals since the nucleation process has been performed previously during the self-nucleation step. This last point will depend on the efficiency of the self-nucleation treatment and therefore on the T_s employed.

Even though self-nucleation before isothermal crystallization is a classic method that has been employed to obtain solution single crystals as well as to study bulk crystallization and nucleation kinetics,[54,62] this is the first time, as far as the authors are aware, that the technique has been applied by DSC in the bulk as a tool to make possible the determination of subsequent isothermal crystallization kinetics.

Selected isothermal DSC scans obtained by quenching (80 °C min^{-1}) the samples to T_c immediately after self-nucleation of neat PPDX[15] at a T_s of 117 °C for 3 min are presented in Fig. 11. It can be seen that at the selected isothermal crystallization temperatures, PPDX[15] did not crystallize during the previous self-nucleation procedure as indicated by the levelling of the baseline after crystallization to a level close to that obtained at the beginning of the scans. The self-nucleation procedure was applied in Domain II where only self-seeds remain, therefore heating DSC scans performed immediately after self-nucleation and quenching to T_c, at equivalent conditions to $t = 0$ min in Fig. 11, exhibited no endothermic signals. This type of check runs was performed in order to ensure that no prior crystallization took place before the isothermal measurements.

Fig. 12a shows a plot of the inverse crystallization half time *versus* T_c for PPDX and for self-nucleated PPDX. The acceleration of the overall crystallization kinetics for the self-nucleated sample is clearly seen by the shift of the curve to higher $1/\tau_{50\%}$ values and higher temperatures. In Fig. 12b plots of $\ln(1/\tau_{50\%}) + U^*/R(T_c - T_\infty)$ *versus* $1/(T_c \Delta Tf)$ according to eqn. (6) for PPDX and self-nucleated PPDX are presented. It can be seen that a good fit is obtained and the values of K_g^τ are presented in Table 2. The results are very satisfactory since the K_g^τ value obtained for neat PPDX is reduced from 31.0 to 17.0 ($\times 10^4$ K^2) once the self-nucleation treatment is performed before the isothermal crystallization. This indicates that the energy barrier for nucleation and growth has been reduced by performing the nucleation in a previous step. A value of $K_g^G = 17.2 \times 10^4$ K^2 is obtained from fitting the Lauritzen and Hoffman theory to spherulitic growth rate experiments in PPDX[15], this value is in remarkably close agreement to the K_g^τ value obtained after self-nucleation has been performed and therefore corresponding to mostly crystal growth. As expected, the values of the fold surface free energy and the work to fold the chains obtained for self-nucleated PPDX[15] are also in close agreement with those obtained for neat PPDX[15] from the application of the Lauritzen and Hoffman theory to spherulitic growth rate data. This agreement indicates that the efficiency of the previous self-nucleation of PPDX[15] at $T_s = 117$ °C within Domain II was very high.

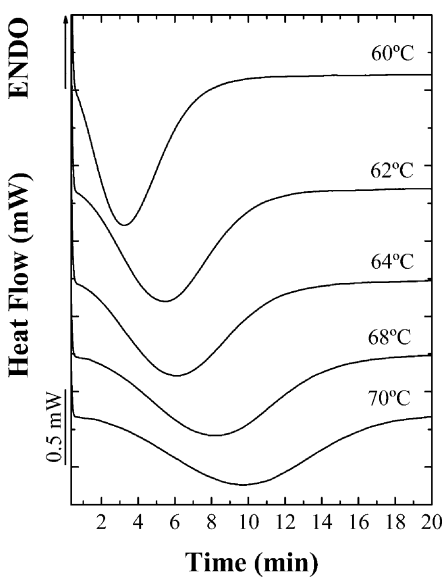

Fig. 11 Examples of DSC isothermal crystallization scans for the PPDX block within $D_{77}^{32}C_{23}^{10}$ diblock copolymer. The measurements are performed after the PPDX block had been previously self-nucleated at $T_s = 110$ °C and then quenched (80 °C min^{-1}) to the indicated T_c temperatures.

Fig. 12 also shows data for two block copolymers whose PPDX block was first self-nucleated and then isothermally crystallized in the DSC. In this case, the molten PCL block covalently attached to the PPDX block slows down the overall crystallization rate, this result being consistent with those presented above in the section of spherulitic growth rate. The higher the PCL content the slower the kinetics for the crystallization of the PPDX block when the two diblock copolymers employed are compared. The fittings to eqn. (6) are also very good in these cases and the values of K_g^{τ} for the PPDX block tend to increase as compared to self-nucleated PPDX[15] as shown in Table 2. As the PCL content in the self-nucleated copolymer increases the values of K_g^{τ}, σ_e and q for the corresponding PPDX block also increase as can be seen in Table 2. For copolymers with higher PCL contents the crystallization kinetics of the PPDX block within the copolymers was so slow that even after self-nucleation the measurements could not be performed.

Our results differ from those obtained previously by Bogdanov *et al.*[40] when they studied by DSC the crystallization kinetics of 80/20 poly(ε-caprolactone)-*b*-(polyethylene glycol) diblock copolymer (PCL-*b*-PEG). In their case, the PCL block crystallized first from a homogeneous melt and the Avrami parameters K and n were found to be similar to the kinetic parameters of the isothermal crystallization of a corresponding PCL homopolymer. A significant crystallization retardation was found for the PEG block that crystallized second. The retardation was attributed to the "mutual influence between the PEG constituent and the PCL crystal phase which fixes (hardened) the total copolymer structure".[40] In our case, conversely, when the PPDX block crystallizes it does so at a slower rate than a comparable PPDX homopolymer. The crystallization of the PCL block, on the other hand, strongly depends on the composition of the diblock copolymer as shown in Fig. 7. However, for $D_{77}^{32}C_{23}^{10}$, the overall kinetics are retarded, which can be regarded as similar to that experienced by the PEG block in the 80/20 PCL-*b*-PEG diblock copolymer studied by Bogdanov *et al.*,[40] the Avrami index in both cases was also of the order of 2.

Recently, Ueda *et al.*[22] have examined the crystallization kinetics of a flow oriented polyethylene-*b*-(atactic polypropylene), PE-*b*-aPP, with a polyethylene volume fraction 0.48. In this case, the crystallization of the PE block occurs with a molten aPP block covalently bonded to it. The components are reported to be in the strong segregation limit and therefore phase separated well before crystallization. They found that the crystallization kinetics (as determined by small angle light scattering) was substantially retarded as compared to an equivalent molecular weight homo-PE. They attributed the effect to a mobility reduction for the chains close to the interfacial region and to the presence of the non-crystallizable aPP chains close to the growth face which could obstruct the growth process. These results are similar to those obtained here for the crystallization of the PPDX block at higher temperatures, when the PCL component is molten. Similar results have been also obtained by Shiomi *et al.*[64] since they have detected a reduction in crystallization rate

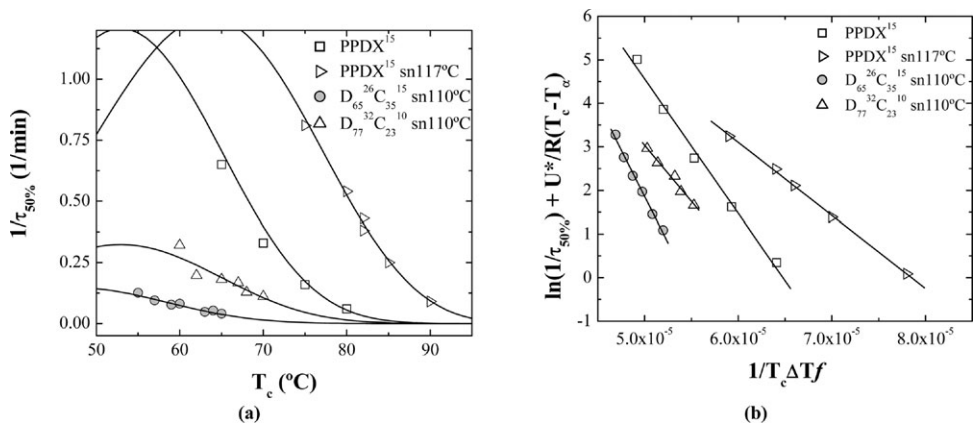

Fig. 12 (a) Inverse of the crystallization half-time as a function of isothermal crystallization temperature for PPDX[15], self-nucleated PPDX[15] and self-nucleated PPDX block within the indicated diblock copolymers. Solid lines are fits to Lauritzen and Hoffman theory according to eqn. 6. (b) Lauritzen and Hoffman kinetic theory plots for the same materials presented in (a).

when they compared a poly(ethylene glycol) homopolymer, PEG, with the PEG block within PEG-*b*-PB diblock copolymers. In this case, the crystallization of the PEG block is carried out with a covalently bonded rubbery block and similar energetic restrictions for its crystallization decrease its crystallization rate as compared to homo-PEG.

The results presented in this paper show for the first time a quantitative measure of the energetic restrictions imposed by the molten PCL block on the crystallization kinetics of the PPDX block within PPDX-*b*-PCL diblock copolymers. As a result of these energetic restrictions the PPDX-*b*-PCL diblock copolymers crystallize at a much slower rate than PPDX homopolymer in the temperature range where only the PPDX can crystallize. This reduction in crystallization rate is the responsible for the coincident crystallization phenomenon experienced by the materials when they are cooled from the melt as in Fig. 1.

The preceding sections have shown the complex influence exerted by one block on the other, such that the nucleation and crystallization kinetics of the material are affected. At temperatures where the PCL block is molten, the PPDX block within PPDX-*b*-PCL diblock copolymers encounters complex changes in its interfacial area as compared to a homo-PPDX that results in a higher energy barrier for growth. Once the PPDX block crystallizes, it nucleates the PCL block. Nevertheless, the PCL block also encounters energetic restrictions for secondary nucleation that are more pronounced as the PPDX content in the copolymer increases.

Finally, some preliminary results on the hydrolytic degradation of $PPDX^{15}$ and two PPDX-*b*-PCL diblock copolymers have been examined. $PPDX^{15}$ completely degrades within a 6 month period. However, when the diblock copolymer containing just 23% PPDX is examined, the degradation rate is substantially reduced as compared to $PPDX^{15}$. A further increase in the PCL content to 35% greatly increases stability. A comparison of weight retention values after 6 months of exposure to the hydrolysis medium reveals that while $PPDX^{15}$ has been completely degraded, $D_{65}^{26}C_{35}^{15}$ has only lost 10% of its weight. The complex dependence of hydrolysis rate on composition derives from the different attack rates on the different phases. Hydrolysis reactions are faster in the amorphous regions of PPDX where water penetration is also faster, and slower in the crystalline regions.[1,2] The access to such regions will also be hindered by the disposition of the PCL lamellae and amorphous regions within the mixed spherulites in the copolymer, since PCL will offer protection against hydrolysis to the material in view of its much greater resistance to it.

Conclusions

AFM observations performed during sequential isothermal crystallization of $D_{23}^{8}C^{27}{}_{77}$ indicate that the final morphology is composed of mixed spherulites where lamellae of both constituents are inter-dispersed. Considering both AFM and POM measurements we can conclude that in PPDX-*b*-PCL diblock copolymers crystallization drives structure formation.

We have applied the Lauritzen and Hoffman kinetic theory to spherulitic growth rate data for PPDX and the PPDX block within $D_{77}^{32}C_{23}^{10}$. The results show that at temperatures higher than 50 °C the spherulitic growth of the PPDX block is energetically hindered by the covalently bonded molten PCL chain, resulting in a much larger fold surface free energy and higher values of the work needed for the chains to fold as compared to homo-PPDX. These energetic restrictions imposed by the molten PCL block on the PPDX are responsible for the coincident crystallization observed when any PPDX-*b*-PCL copolymer is cooled from the melt.

The application of the Lauritzen and Hoffman theory to overall crystallization rate data was highly successful for PPDX and the diblock copolymers. This was corroborated by applying it to data from DSC measurements of isothermal crystallization of previously self-nucleated PPDX and obtaining a perfect match with the energetic parameters determined from spherulitic growth rate data. The use of self-nucleation allowed the determination of the overall crystallization kinetics of the PPDX block within two copolymers (with 65 and 77% PPDX) which was otherwise too slow for detection. The results indicate that the energetic restrictions for the crystallization of the PPDX block at high temperatures increase as the PCL content in the copolymer increases.

In the case of the PCL block, the overall crystallization kinetics was determined after PPDX was crystallized until saturation. PPDX was found to nucleate PCL accelerating the overall kinetics of the PCL block within diblock copolymers with 60 and 77% PCL. When the PCL content was lower than 50%, a reduction in crystallization rate as well as a reduction in the Avrami index indicated

that the previously crystallized PPDX (which is the matrix in these cases) was imposing some topological restrictions on the PCL block. Nevertheless, the crystallization was always heterogeneous and in the same undercooling range regardless of composition. The self-nucleation behaviour of the diblock copolymers also indicated that the PPDX within the copolymers is capable of nucleating the PCL and that its nucleation was always heterogeneous, since all three self-nucleation Domains were present. Through self-nucleation a separation of the crystallization exotherms of PPDX and PCL during the cooling scan in the DSC can be achieved.

Acknowledgements

The Simón Bolívar University team acknowledges sponsorship by Fonacit, through grant S1-2001000742. Discussion with Drs. Arnal and Balsamo from Simón Bolívar University Polymer Group are gratefully acknowledged. LPCM members are very grateful to "Région Wallonne" and European Community (FEDER, FSE) for general support in the frame of "Objectif 1-Hainaut: Materia Nova". This work was partly supported by the Belgian Federal Government Office of Science Policy (SSTC-PAI 5/3). J.-M. Raquez is Scientific Research Collaborator of the Belgian F.N.R.S.

References

1 R. S. Bezwada, D. D. Jamiolkowski and K. Cooper, in *Handbook of Biodegradable Polymers*, eds. A. J. Domb, J. Kost and D. M. Wiseman, Harwood, Singapore, 1997, ch. 2, pp. 29–61.
2 M. A. Sabino, J. Albuerne, A. J. Müller, J. Brisson and R. E. Prud'homme, *Biomacromolecules*, 2004 **5**, 358.
3 P. Rangarajan, R. A. Register and L. J. Fetters, *Macromolecules*, 1993, **26**, 4640.
4 P. Rangarajan, R. A. Register, D. H. Adamson, L. J. Fetters, W. Bras, S. Naylor and A. J. Ryan, *Macromolecules*, 1995, **28**, 1422.
5 A. J. Ryan, I. W. Hamley, W. Bras and F. S. Bates, *Macromolecules*, 1995, **28**, 3860.
6 P. H. Richardson, R. W. Richards, D. J. Blundell, W. A. MacDonald and P. Mills, *Polymer*, 1995, **36**, 3059.
7 D. J. Quiram, R. A. Register, G. R. Marchand and A. J. Ryan, *Macromolecules*, 1997, **30**, 8338.
8 K. C. Douzinas, R. E. Cohen and A. F. Halasa, *Macromolecules*, 1991, **24**, 4457.
9 I. W. Hamley, J. Patrick, A. Fairclough, N. J. Terrill, A. J. Ryan, P. M. Lipic, F. S. Bates and E. Towns-Andrews, *Macromolecules*, 1996, **29**, 8835.
10 P. Rangarajan, R. A. Register, L. J. Fetters, W. Bras, S. Taylor and A. J. Ryan, *Macromolecules*, 1995, **28**, 4932.
11 S. Nojima, K. Kato, S. Yamamoto and T. Ashida, *Macromolecules*, 1992, **25**, 2237.
12 D. J. Quiram, R. A. Register, G. R. Marchand and A. J. Ryan, *Macromolecules*, 1997, **30**, 4551.
13 A. Rohadi, R. Endo, S. Tanimoto, S. Sasaki and S. Nojima, *Polym. Int*., 2000, **32**, 602.
14 A. Rohadi, S. Tanimoto, S. Sasaki and S. Nojima, *Polym. J*., 2000, **32**, 859.
15 A. J. Ryan, J. P. A. Fairclough, I. W. Hamley, S.-M. Mai and C. Booth, *Macromolecules*, 1997, **30**, 1723.
16 M. A. Hillmyer and F. S. Bates, *Macromol. Symp*., 1997, **117**, 121.
17 Y.-L. Loo, R. A. Register and A. J. Ryan, *Macromolecules*, 2002, **35**, 2365.
18 S. Nojima, M. Toei, S. Hara, S. Tanimoto and S. Sasaki, *Polymer*, 2002, **43**, 4087.
19 G. Reiter, G. Castelein, J.-U. Sommer, A. Röttele and T. Thurn-Albrecht, *Phys. Rev. Lett*., 2001, **87**, 226 101.
20 C. Robitaille and J. Prud'homme, *Macromolecules*, 1983, **16**, 665.
21 D. J. Quiram, R. A. Register, G. R. Marchand and D. H. Adamson, *Macromolecules*, 1998, **31**, 4891.
22 M. Ueda, K. Sakurai, S. Okamoto, D. Lohse, W. J. MacKnight, S. Shinkai, S. Sakurai and S. Nomura, *Polymer*, 2003, **44**, 6995.
23 G. Reiter, *J. Polym. Sci.: Part B: Polym. Phys*., 2003, **41**, 1869.
24 *Polymer Crystallization, Observations, Concepts and Interpretations*, ed. J. U. Sommer and G. Reiter, Springer, Berlin, 2003.
25 A. J. Müller, V. Balsamo, M. L. Arnal, T. Jakob, H. Schmalz and V. Abetz, *Macromolecules*, 2002, **35**, 3048.
26 M. L. Arnal, V. Balsamo, F. López-Carrasquero, J. Contreras, M. Carrillo, H. Schmalz, V. Abetz, E. Laredo and A. J. Müller, *Macromolecules*, 2001, **34**, 7973.
27 G. Floudas and C. Tsitsilianis, *Macromolecules*, 1997, **30**, 4381.
28 M. Gervais and B. Gallot, *Polymer*, 1981, **22**, 1129.
29 B. Lotz and A. J. Kovacs, *Polym. Prepr. (Am. Chem. Soc., Div. Polym. Chem.)*, 1969, **10**, 820.
30 J. J. J. O'Malley, *Polym. Sci., Polym. Symp*., 1977, **60**, 151.

31 L. Zhu, Y. Chen, A. Zhang, B. H. Calhoun, M. Chun, R. P. Quirk, S. Z. D. Cheng, B. S. Hsiao, F. Yeh and T. Hashimoto, *Phys. Rev. B*, 1999, **60**, 10 022.
32 L. Zhu, S. Z. D. Cheng, B. H. Calhoun, Q. Ge, R. P. Quirk, E. L. Thomas, B. S. Hsiao, F. Yeh and B. Lotz, *Polymer*, 2001, **42**, 5829.
33 L. Zhu, B. R. Mimnaugh, Q. Ge, R. P. Quirk, S. Z. D. Cheng, E. L. Thomas, B. Lotz, B. S. Hsiao, F. Yeh and L. Liu, *Polymer*, 2001, **42**, 9121.
34 L. Zhu, S. Z. D. Cheng, P. Huang, Q. Ge, R. P. Quirk, E. L. Thomas, B. Lotz, B. S. Hsiao, F. Yeh and L. Liu, *Adv. Mater*., 2002, **14**, 31.
35 L. Zhu, P. Huang, W. Y. Chen, Q Ge, R. P. Quirk, S. Z. D. Cheng, E. L. Thomas, B. Lotz, B. S. Hsiao, F. Yeh and L Liu, *Macromolecules*, 2002, **35**, 3553.
36 J. T. Xu, J. J. Yuan and S. Y. Cheng, *Eur. Polym. J*., 2003, **39**, 2091.
37 P. A. Weimann, D. A. Hajduk, C. Chu, K. A. Chaffin, J. C. Brodil and F. S. Bates, *J. Polym. Sci.: Part B: Polym. Phys*., 1999, **37**, 2053.
38 Y. L. Loo, R. A. Register, A. J. Ryan and G. T. Dee, *Macromolecules*, 2001, **34**, 8968.
39 Y. K. Choi, Y. H. Bae and S. W. Kim, *Macromolecules*, 1998, **31**, 8766.
40 B. Bogdanov, A. Vidts and H. Berghmans, *Macromolecules*, 1999, **32**, 726.
41 Y. Wang and M. Hillmyer, *J. Polym. Sci.: Part A: Polym. Chem*., 2001, **39**, 2755.
42 J. Albuerne, L. Márquez, A. J. Müller, J. M. Raquez, Ph. Degée, Ph. Dubois, V. Castelletto and I. W. Hamley, *Macromolecules*, 2003, **36**, 1633.
43 R. M. Ho, P. Y. Hsieh, W. H. Tseng, C. C. Lin, B. H. Huang and B. Lotz, *Macromolecules*, 2003, **36**, 9085.
44 A. J. Müller, J. Albuerne, L. M. Esteves, L. Márquez, J. M. Raquez, Ph. Degée, Ph. Dubois, S. Collins and I. W. Hamley, *Macromolecular Symp*., 2004, in press.
45 N. Bhattarai, H. Y. Kim, D. I. Cha, D. R. Lee and D. I. Yoo, *Eur. Polym. J*., 2003, **39**, 1365.
46 J.-M. Raquez, P. Degée, R. Narayan and P. Dubois, *Macromol. Rapid Commun*., 2000, **21**, 1063.
47 A. Lendlein and L. Langer, *Science*, 2002, **296**, 1673.
48 J. K. Hobbs, A. D. L. Humphris and M. J. Miles, *Macromolecules*, 2001, **34**, 5508.
49 B. Fillon, J. C. Wittmann, B. Lotz and A. Thierry, *J. Polym. Sci., Part B: Polym. Phys*., 1993, **31**, 1383.
50 V. Castillo, A. J. Müller and M. Hillmyer, 2004, unpublished results.
51 M. A. Sabino, J. L. Feijoo and A. J. Müller, *Macromol. Chem. Phys*., 2000, **201**, 2687.
52 J. I. Lauritzen Jr. and J. D. Hoffman, *J. Appl. Phys*., 1973, **44**, 4340.
53 *Physical Properties of Polymers Handbook*, ed. J. E. Mark, AIP Press, New York, 1996.
54 J. Schultz, *Polymer Crystallization*, American Chemical Society, Washington, 2001.
55 S. Andjelic, D. Jamiolkowski, J. Mcdivitt, J. Fischer, J. Zhou and R. Vetrecin, *J. Appl. Polym. Sci*., 2001, **79**, 742.
56 M. Avrami, *J. Chem. Phys*., 1939, **7**, 1103; M. Avrami, *J. Chem. Phys*., 1940, **8**, 212; M. Avrami, *J. Chem. Phys*., 1941, **9**, 177.
57 L. Mandelkern, in *The Crystalline State*, eds. J. E. Mark, A. Eisenberg, W. W. Graessley, L. Mandelkern and J. L. Koenig, *Physical Properties of Polymers*, 2nd edn., ACS, Washington, 1993.
58 W. S. Lambert and P. J. Phillips, *Macromolecules*, 1994, **27**, 3537.
59 V. Balsamo, Y. Paolini, G. Ronca and A. J. Müller, *Macromol. Chem. Phys*., 2000, **201**, 2711.
60 H. Schmalz, A. J. Müller and V. Abetz, *Macromol. Chem. Phys*., 2003, **204**, 111.
61 M. L. Arnal, F. López-Carrasquero, E. Laredo and A. J. Müller, *Eur. Polym. J*., 2004, **40**, 1461.
62 B. Wunderlich, *Macromolecular Physics, Volume 2, Crystal Nucleation, Growth, Annealing*, Academia Press, New York, 1976, pp. 52–70.
63 *Polymer Handbook*, ed. J. Brandrup, E. H. Immergut, E. A. Grulke, A. Abe and D. R. Bloch, 4th edn., John Wiley and Sons, New York, 1999.
64 T. Shiomi, H. Takeshita, H. Kawaguchi, M. Nagai, K. Takenaka and M. Miya, *Macromolecules*, 2002 **35**, 8056.